Visible-IR and Raman microspectroscopic investigation of three Itokawa particles collected by Hayabusa: Mineralogy and degree of space weathering based on nondestructive analyses

L. Bonal, R. Brunetto, P. Beck, E. Dartois, Z. Dionnet, Z. Djouadi, J. Duprat, E. Füri, Y. Kakazu, G. Montagnac, et al.

The Meteoritical Society

Meteoritics & Planetary Science 50, Nr 9, 1562–1576 (2015)
doi: 10.1111/maps.12496

Visible-IR and Raman microspectroscopic investigation of three Itokawa particles collected by Hayabusa: Mineralogy and degree of space weathering based on nondestructive analyses

L. BONAL[1*], R. BRUNETTO[2], P. BECK[1], E. DARTOIS[2], Z. DIONNET[2], Z. DJOUADI[2], J. DUPRAT[3], E. FÜRI[4], Y. KAKAZU[3], G. MONTAGNAC[5], P. OUDAYER[2], E. QUIRICO[1], and C. ENGRAND[3]

[1]Institut de Planétologie et d'Astrophysique de Grenoble, CNRS/UJF Grenoble 1, Grenoble 38041, France
[2]Institut d'Astrophysique Spatiale, CNRS/Université Paris Sud, Orsay F-91405, France
[3]Centre de Sciences Nucléaires et de Sciences de la Matière, CNRS/Université Paris Sud, Orsay F-91405, France
[4]Centre de Recherche Pétrographiques et Géochimiques, CNRS, Nancy 54501, France
[5]Laboratoire de Géologie de Lyon, Terre, Planètes, Environnement—ENS Lyon—6 allée d'Italie, 69364, Lyon Cedex 07, France
[*]Corresponding author. E-mail: lydie.bonal@obs.ujf-grenoble.fr

(Received 24 October 2014; revision accepted 28 June 2015)

Abstract–Hayabusa-returned samples offer a unique perspective for understanding the link between asteroids and cosmomaterials available in the laboratory, and provide insights on the early stages of surface space weathering. This study characterizes the mineralogy and the extent of space weathering of the three Itokawa particles RA-QD02-0163, RA-QD02-0174, and RA-QD02-0213 provided by JAXA to our consortium. We report here a series of results based on nondestructive analyses through visible-near-infrared reflectance and Raman spectroscopy. Results were obtained on the raw particles, both in their original containers and deposited on diamond windows. Identification of the minerals, characterization of their elemental compositions, and measurements of their relative abundances were led through Raman spectroscopy in punctual and automatic mode. Reflectance spectra in the visible and near-IR wavelengths constrain the mineralogy of the grains and allow direct comparison with the surface of Itokawa. The spectra reflect the extent of space weathering experienced by the three particles. Particle RA-QD02-0163 consists of a heterogeneous mixture of minerals: olivine (Fo_{76}) dominates an assemblage with both Ca-rich (En_{50}, Wo_{50}) and Ca-poor (En_{85}) pyroxenes. The elemental compositions of the silicates are consistent with those previously reported for distinct Hayabusa particles. Particles RA-QD-0174 and RA-QD02-0213 are solely composed of olivine, whose chemical composition is similar to that observed in RA-QD02-0163. It has been previously shown that the S-type asteroid 25143 Itokawa is a breccia of poorly equilibrated LL4 and highly equilibrated LL5 and LL6 materials. The three particles studied here can be related to the least metamorphosed lithology (LL4) based on the high forsterite content of the olivine. Neither carbonaceous matter nor hydrated minerals were detected through Raman on the three allocated particles. The NIR-VIS reflectance (incidence = 45°, light collection at e = 0°) spectra of the three particles, in particular the 1 μm band, are consistent with the presence of both olivine and pyroxene detected via Raman. The spectra of particles RA-QD02-0163 and RA-QD02-0213 are also fully compatible with the ground-based observations of asteroid (25143) Itokawa in terms of both spectral features and slope. By contrast, particle RA-QD02-0174 has a similar 1 μm band depth but higher (redder) spectral slope than the surface of Itokawa. This probably reveals a variable extent of space weathering among the regolith particles. RA-QD02-0174 may contain a higher amount of nanophase metallic iron and nanophase FeS. Such phases are products by space weathering induced by solar wind, previously detected on other Itokawa particles.

INTRODUCTION

The Hayabusa spacecraft was launched by JAXA on May 9th, 2003 and reached the S-type asteroid (25143) Itokawa in September 2005. Remote sensing analyses were carried out around Itokawa for several months to characterize its shape, surface topography, color, composition, and density. Based on near-infrared and X-ray fluorescence spectra, it was shown that Itokawa is mainly composed of olivine and is related to LL5-6 ordinary chondrites (e.g., Abe et al. 2006; Fujiwara et al. 2006; Okada et al. 2006), in agreement with previous ground-based measurements (e.g., Binzel et al. 2001; Lederer et al. 2005; Lowry et al. 2005; Abell et al. 2007). Hayabusa carried out two touchdowns in the smooth terrain of MUSES-C Regio to sample the regolith layer in November 2005 (Yano et al. 2006). The reentry capsule was recovered on Earth in June 2010 (Yada et al. 2014) and more than a thousand asteroidal particles were collected, offering a unique perspective to better constrain the connection between asteroids and cosmomaterials available in the laboratory and to provide an insight on surface space weathering. After being studied by pre-examination teams, Itokawa particles are now being characterized by various research groups following an international announcement of opportunity (e.g., Yada et al. 2014).

The thorough and multi-analytical preliminary examination of approximately 40 particles suggests that the samples are LL chondrite materials based on the mineralogy, and modal and elemental abundances of minerals (Nakamura et al. 2011); bulk density and 3-D structures (Tsuchiyama et al. 2011); and oxygen isotopic compositions of olivine, orthopyroxene, and plagioclase minerals (Yurimoto et al. 2011) present in the samples. Based on textures, chemical compositions (more or less equilibrated), and relative abundances of major minerals, the thermal history of the grains was constrained: most of the particles (~90%) are similar to LL5 and LL6 chondrites. The remaining particles (~10%) appear similar to LL4 chondrites (Nakamura et al. 2011; Tsuchiyama et al. 2011). More details on the thermal history of ordinary chondrites can be found in the papers by Van Schmus and Wood (1967), Rubin (1990) and a review by Brearley and Jones (1998).

The surface of an atmosphere-less body exposed to interplanetary space has its structures, optical properties, chemical compositions, and mineralogy gradually changed by irradiation; implantation; and sputtering by solar wind, galactic cosmic ions, electrons, UV and X-rays; and bombardment by micrometeorites (e.g., Clark et al. 2002; Chapman 2004; Domingue et al. [2014] and references therein). The surface alteration varies with the location in the solar system and the timing in solar system history (e.g., Chapman 2004). However, until the surface material of the asteroid Itokawa was returned to Earth by the Hayabusa spacecraft, our knowledge of space weathering was mainly based on Apollo samples returned from the surface of the Moon (see Hapke [1993] and references therein), on regolith breccia meteorites (e.g., Keil 1982; Clark et al. 2002; Basu and McKay 1983; McKay et al. 1991; Noble et al. 2010), as well as on laboratory simulations of space weathering processes (e.g., Cassidy and Hapke 1975; Dukes et al. 1999; Yamada et al. 1999; Sasaki et al. 2001; Strazzulla et al. 2005; Brunetto et al. 2006a; Loeffler et al. 2009). Lunar studies revealed spectral changes in the visible to near-infrared resulting from space weathering that include darkening of the albedo, reddening of the reflectance spectra, and attenuation of the absorption bands. In the UV space weathering brightens, creates bluing of the spectrum, and degrades the near- and mid-UV absorption edge (Hendrix and Vilas 2006; Hendrix et al. 2012). The key role played by production of nanophase metallic iron ($npFe^0$) due to vapor condensation from micrometeorite impacts and surface sputtering was established (Keller and McKay 1993, 1997; Wentworth et al. 1999; Keller et al. 2000; Pieters et al. 2000; Taylor et al. 2001; Hapke 2001).

Fundamental reviews on space weathering have been published: the reader is invited to refer to Hapke (2001), Clark et al. (2002), and Chapman (2004), for a comprehensive view of the state of the art about one decade ago. At that time, the main effects of space weathering and the basics of the asteroid–meteorite connection had already been settled, mainly thanks to the lunar studies, to asteroid remote sensing spectroscopy, and to observations by Galileo and NEAR spacecrafts (Chapman 1996; Clark et al. 2002). For a more recent review on space weathering, see Gaffey (2010), Bennett et al. (2013), and Brunetto et al. (2015). Better knowledge of asteroidal space weathering can provide clues to further constrain the relation between asteroid taxonomical classes and meteorite classes. The case of S-type asteroids versus ordinary chondrites has been particularly studied: by comparing ordinary chondrites to main-belt S-types through near-Earth asteroids a VIS-NIR reddening spectral trend is observed (Binzel et al. 2004; Lederer et al. 2005; Marchi et al. 2005). The study of young asteroid families strongly suggests a reddening trend with respect to space exposure, illustrating the major role played by the solar wind ions (Brunetto et al. 2006a; Marchi et al. 2006; Willman et al. 2008; Vernazza et al. 2009). In particular, Vernazza et al. (2009) showed the existence

of two different regimes of space weathering; the first one being very rapid (<0.5 Myr) is essentially attributed to the solar wind irradiation effects, and the micrometeorite impacts may play a role in the second one that is more gradual (evolution over the interval t = 0.5–5 Ma to t = 2500 Ma). Nesvorny et al. (2010) considered the effect of encounters of NEAs with all terrestrial planets: the observed fraction of Q-type NEAs can be used to constrain the space weathering time scale and the encounter radius below which the refreshing effect occurs. They confirmed that the space weathering time scale is shorter than 10^6 yr. Spectrometers onboard Hayabusa showed variable intensity of space weathering effects across different regions of the asteroid Itokawa (Abe et al. 2006; Hiroi et al. 2006; Ishiguro et al. 2007). Therefore, Itokawa particles are providing unique clues to investigate asteroidal space weathering. Various lines of evidence for space weathering were reported: distinct types of surface modification and presence of Fe-rich and FeS nanoparticles (Noguchi et al. 2011, 2014), solar wind implantation (Nagao et al. 2011), and grain surface erosion (Tsuchiyama et al. 2011). Noguchi et al. (2014) identified three types of surface modification, probably formed by space weathering at the surfaces of Itokawa particles. Although micrometeorite impact may have played a role in the formation of the uppermost zone, textures strongly suggest that solar wind irradiation damage and implantation are the major causes of surface modification and space weathering on Itokawa. Noguchi et al. (2014) concluded on the absence of major role for micrometeorite impact that the surface modifications observed on the Itokawa particles might be mostly related to solar wind irradiation and implantation. The studies on Hayabusa particles confirm the reddening and darkening of asteroids due to space weathering. The residence time of the grains at the surface of Itokawa is probably short (around 1.5 Myr) as inferred by noble gases isotopes, and in particular on the abundance of cosmic-ray-produced ^{21}Ne (Nagao et al. 2011; Meier et al. 2014). Solar flare track densities in Hayabusa particles led Keller and Berger (2014) and Noguchi et al. (2014) to conclude on a much shorter residence time ranging from $<10^3$ to 3×10^4 yr. The Hayabusa mission thus provides new and significant progress in terms of understanding space weathering of relatively young asteroidal surfaces.

The scientific objectives of the work presented here are to characterize the asteroidal geological alteration and surface processes (e.g., space weathering alteration) as revealed by the Itokawa grains. We report results based on nondestructive visible-NIR, and Raman spectroscopy of three Itokawa particles (RA-QD02-0163, RA-QD02-0174, and RA-QD02-0213) allocated by JAXA to our consortium. In particular, the collection of visible-NIR reflectance spectra of these asteroidal grains provides an interesting approach to support remote sensing spectral characterization of asteroids and provides a bridge between astronomical observations and geochemical analyses of natural samples of extraterrestrial origin.

EXPERIMENTAL TECHNIQUES

Sample Preparation

Our objective was to characterize the three allocated Hayabusa particles without altering them. The results were thus obtained on raw particles, both (i) in the original sealed containers designed by JAXA (under nitrogen atmosphere), and (ii) deposited in a commercial compression cell commonly used in IR spectroscopy. The cell (Diamond "EX-press") is made of two 2 mm diameter synthetic type II diamond windows. The choice of transferring the grains into individual diamond cells was justified by the compatibility of the cell with the optical techniques chosen to characterize the grains. Indeed, Raman spectroscopy and VIS-NIR reflectance spectroscopy can be run after opening the cell to remove the upper diamond window (see Dartois et al. [2013] for more details on the experimental protocol used on the same type of cell). To prevent crushing of the Hayabusa grains between the two diamond windows, the cell was slightly modified with an inside gasket on the lower diamond window. As this gasket is higher than the thickness of the individual grains, it prevented damaging them when closing the cell. In a second step, the Hayabusa particle RA-QD02-0163 was manually transferred, under Earth's atmosphere, from the original container to the lower diamond window with a pencil wet in water under a binocular microscope in a laminar flow in a clean room to prevent contamination due to terrestrial grains. The same procedure was followed up for particles RA-QD02-0174 and RA-QD02-0213 except that a dry, instead of wet, pencil was used. The samples were all stored in a vacuum desiccator. The considered particles are all minerals related to equilibrated ordinary chondrite. With the analytical technique used in present work we investigate bulk particles at the scale of several microns. We are thus not sensitive to the potential oxidation effects evoked by Noguchi et al. (2014) on FIB sections.

Spectral Analysis

Raman microspectroscopy was performed on the three grains in their original holders by using a DXR™ Raman microspectrometer from Thermo Fisher with a

532 nm exciting laser radiation available on the SMIS beamline (spectroscopy and microscopy in the infrared using synchrotron; Dumas et al. 2006) at SOLEIL. The laser spots were 2 μm in diameter at the surface of the sample, and the power on the sample was lower than 0.3 mW, producing power densities lower than 100 W mm^{-2} to prevent damage on the sample (similar values were used by Brunetto et al. [2011] on an interplanetary dust particle of similar size as the Itokawa particles and proved to be low enough not to alter the sample). A spectral resolution of 4 cm^{-1} and a spatial resolution of about 1 μm were used. Point analyses and automatic mapping were performed.

Itokawa particles RA-QD02-0213 and RA-QD02-0173 are monomineralic. Additional Raman analyses were thus only carried out on Itokawa particle RA-QD02-0163 after it was transferred into the diamond cell. These measurements were performed at the Laboratoire de Géologie de Lyon (Université Claude Bernard—Ecole Normale Supérieure de Lyon, France). We used a LabRam Raman spectrometer (Horiba Jobin-Yvon) equipped with a 600 g mm^{-1} grating and a Spectra Physics Ar + laser provided a 514 nm excitation wavelength. The calibration of the spectrometer was verified on a silicon wafer at the beginning of every measurement session. The laser beam was focused through a long focal distance ×50 objective, leading to a ~1.5 μm circular spot. The power on the samples was typically 1 mW, producing power densities of the order of 500 W mm^{-2}. The absence of laser damage was checked visually on the camera image and spectroscopically through reproducibility tests. Point analyses and automatic mapping were performed. The mapping of the grain surface was carried out with an autofocus mode. Each acquisition consisted of two integrations over 5 s along a 1 μm grid pattern, ensuring a signal-to-noise ratio high enough to identify the mineral phases and to resolve them spatially without oversampling. Spectra of individual minerals were also acquired. The acquisition time was longer (t_{acq} = 60 s) to optimize the signal-to-noise ratio. Spectra, for the automatic mapping and point analyses, were all acquired in the 160–1960 cm^{-1} spectral range.

Visible-NIR (0.4–1.0 μm) reflectance microspectroscopy was performed at Orsay (see Brunetto et al. [2014] for more details) using a VIS-NIR grating spectrometer Maya2000 Pro (Ocean Optics), coupled through infrared transparent fibers to an optical microscope, allowing illumination at angles higher than 35° (i = 45° was used) and light collection at a fixed angle e = 0°. The size of the illumination spot on the sample surface was ~50 μm and ~20 μm for ×20 and ×50 objectives, respectively. The sample was placed horizontally and its vertical position was adjusted by maximizing the reflectance signal corresponding to the best focalization of the optical image. Reference spectra were collected with respect to a 99% Spectralon standard (Labsphere) and double-checked using a $BaSO_4$ standard. The spectral resolution was fixed at 1 nm.

RESULTS

Preliminary secondary electron images acquired by the JAXA team (Fig. 1) indicate that RA-QD02-0163 is a 30 μm wide particle. RA-QD02-0174 and RA-QD02-0213 are irregular and slightly bigger with apparent diameters of 54 μm.

Raman

Particle RA-QD02-0163

The particle RA-QD02-0163 is composed of olivine and pyroxene (Fig. 2). No plagioclase was detected, nor oxides, in contrast to other Hayabusa particles (e.g., Nakamura et al. 2011; Tsuchiyama et al. 2011; Yurimoto et al. 2011). Raman spectroscopy is highly sensitive to the presence of polyaromatic carbonaceous material. The main carbon bands are visible in the (1000–1800 cm^{-1}) spectral range. The nonobservation of carbon Raman bands thus clearly attests the absence of carbonaceous material in particle RA-QD02-0163.

Raman spectra of olivine are characterized by the presence of a doublet in the 815–860 cm^{-1} spectral region. The frequencies of both peaks are shifting along the cation substitution between forsterite and fayalite. We estimated the chemical composition of olivine from Raman spectra using the calibration established by Kuebler et al. (2006). The olivine in particle RA-QD02-0163 has a homogeneous Mg-rich composition, equivalent to $Fo_{76\pm5}$.

The major-element composition of the Mg-, Fe-, Ca-pyroxenes can be semiquantitatively determined on the basis of the peak positions of their characteristic Raman modes using the calibration established by Huang et al. (2000). The inferred chemical compositions for clinopyroxene in particle RA-QD02-0163 are such as En_{50}, Wo_{50}. The Ca-poor pyroxene is such as En_{85}.

The Raman mapping (Fig. 3) shows that olivine (in red), clinopyroxene (in green), and orthopyroxene (in blue) are several micrometers wide minerals. Olivine slightly dominates in size.

Particles RA-QD02-0174 and RA-QD02-0213

Particles RA-QD02-0174 and RA-QD02-0213 are monomineralic grains. They are both only composed of olivine (Fig. 4). Similar to RA-QD02-0163, the chemical compositions of olivine were estimated from their

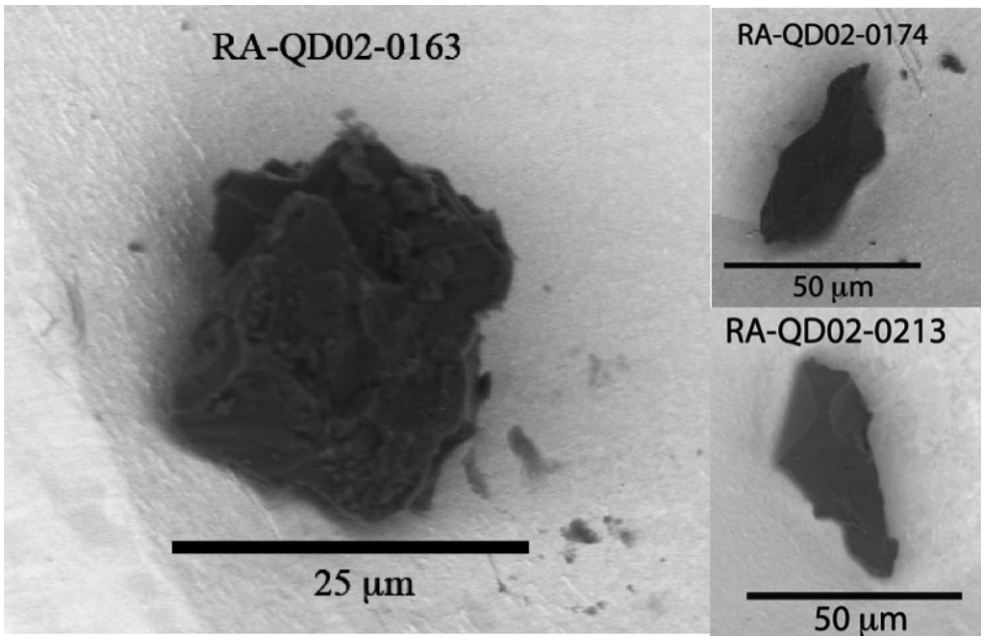

Fig. 1. Backscattered images of RA-QD02-0163, RA-QD02-0174, and RA-QD02-0213. These images were kindly provided by JAXA.

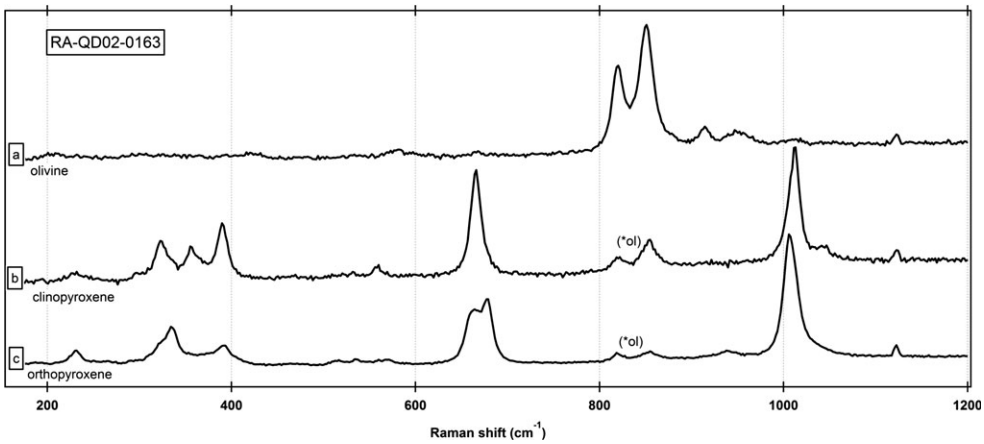

Fig. 2. Raman spectra of individual minerals in RA-QD02-0163. The Raman spectra were all normalized to their most intense band. A vertical offset was applied for ease of reading of the figure. The doublet of olivine (*ol) is visible on the pyroxene spectra.

Raman spectra using the calibration established by Kuebler et al. (2006). The olivine minerals in RA-QD02-0174 and RA-QD02-0213 have a homogeneous Mg-rich composition, equivalent to $Fo_{76\pm5}$.

VIS-NIR

The reproducibility of VIS-NIR reflectance spectroscopy, at the ~20 μm scale, was evaluated through preliminary tests to estimate measurement uncertainty. For calibrations, natural San Carlos olivine 20–100 μm particles were used. The reflectance spectra of isolated particles were measured one by one using different microscope objectives (i.e., different sizes of the analytical spot, from 200 μm down to 20 μm). Olivine grains were deposited on quartz windows, in contrast to Itokawa particles deposited on diamond windows. However, quartz and diamond are two substrates that are transparent in this optical range: they are not characterized by a specific spectral signature. Thus, these two substrates do not modify the reflectance spectra of the considered samples. It is then

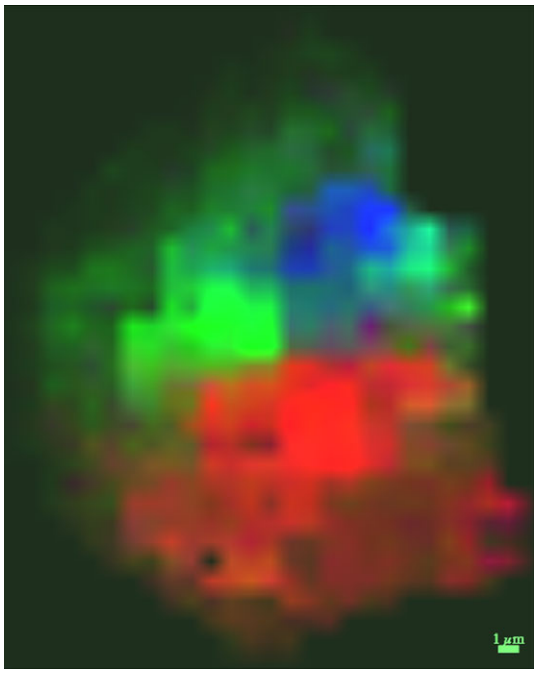

Fig. 3. Raman spectroscopic image of the identified silicates present at the surface of RA-QD02-0163. Olivine, orthopyroxene, and clinopyroxene are shown in red, blue, and green color scales, respectively. The Raman spectrum obtained on each point of the grid has been fitted by a linear combination of the three identified minerals (Fig. 2) through a least squares method. The color scale thus represents the relative abundances of the considered minerals.

possible to apply the measurements uncertainty evaluated from reflectance spectra of individual olivine deposited on quartz to Itokawa particles deposited on diamond windows. Reflectance spectra of San Carlos olivine were also measured in macroscopic conditions (spot size ~1 mm, using the same experimental conditions as Brunetto et al. 2014) on thick (~2 mm) dust deposits. In Fig. 5, the measurements of San Carlos olivine are compared with similar published data. The spectra are all characterized by a comparable spectral shape and band position. The spectral variability (an example in Fig. 5 is provided by the spectrum for a ×20 objective) can essentially be ascribed to the surface roughness and relative angle between grain surface and incident light at the observed spot. Using the range of spectral variations we estimated relative error bars as a function of wavelength (see the gray area in Fig. 5) taking into account an error of 3% due to the fluctuations of the visible source and focal point reproducibility. These relative error bars were applied to infer the uncertainty on the spectra of the Itokawa particles (see below).

The VIS-NIR bidirectional reflectance spectra of particles RA-QD02-0163, RA-QD02-0174, and RA-QD02-0213 (Fig. 6) were measured using the same procedure and geometry as the calibration spectra on San Carlos olivine, using a ×50 objective (the ×20 objective was used to double-check the results). In Fig. 6, the peak positions (retrieved from the literature) of bands M1-1 and M2 of a Fo_{75} olivine (Sunshine and Pieters 1998) and of the large ~0.94 μm band of a mixture 50:50 of orthopyroxene and clinopyroxene (Sunshine et al. 1990) are plotted for comparison with the spectra of Hayabusa particles. The VIS-NIR reflectance spectra are consistent with the presence of the minerals detected by Raman spectroscopy. Particle RA-QD02-0163 is the only one compatible with the presence of pyroxene. Unfortunately, the limited spectral range does not allow for a more detailed study of the 1 μm band. In particular, precise band depth and position cannot be estimated because the right shoulder of the band is missing in our spectra, thus a mineral composition cannot be retrieved from these VIS-NIR data.

The spectra of particles RA-QD02-0163 and RA-QD02-0213 are compatible with the ground-based observations of the asteroid Itokawa (Lowry et al. 2005) in terms of spectral slope (see Fig. 7 and Table 1). In Fig. 6, the 1 μm band of particle RA-QD02-0174 is similar to that observed on particle RA-QD02-0213. This is consistent with the fact that the two particles share an olivine-rich composition (see Raman results). Nevertheless, particle RA-QD02-0174 has a significantly higher (redder) spectral slope and different normalized reflectance (see Table 1). The spectral slopes calculated on the 0.4–0.7 μm range are reported in Table 1. They are obtained through a linear fit of the scaled spectra in the visible range, providing a straightforward way to compare the spectral continuum of different spectra. Lazzarin et al. (2006) reported another slope calculation method, i.e., a linear fit (restricted to the 0.52–0.92 μm range) on spectra scaled to 1 at 0.55 μm. The latter method provides a slope that depends both on the spectral continuum and on the 1 μm band depth and position, and thus is not only sensitive to the space weathering effects but also to the mineralogy. The Lazzarin et al. (2006) method has been used to characterize large spectroscopic surveys of asteroids. We compare both in Table 1.

DISCUSSION

Hayabusa Particles: Grains Representative of Itokawa's Surface Available in Laboratory

Mineral Characterization

Similar to the large majority of Hayabusa particles, RA-QD02-174 and RA-QD02-213 are monomineralic (Nakamura et al. 2011). They are solely composed of olivine. RA-QD02-163 is the only polymineralic particle

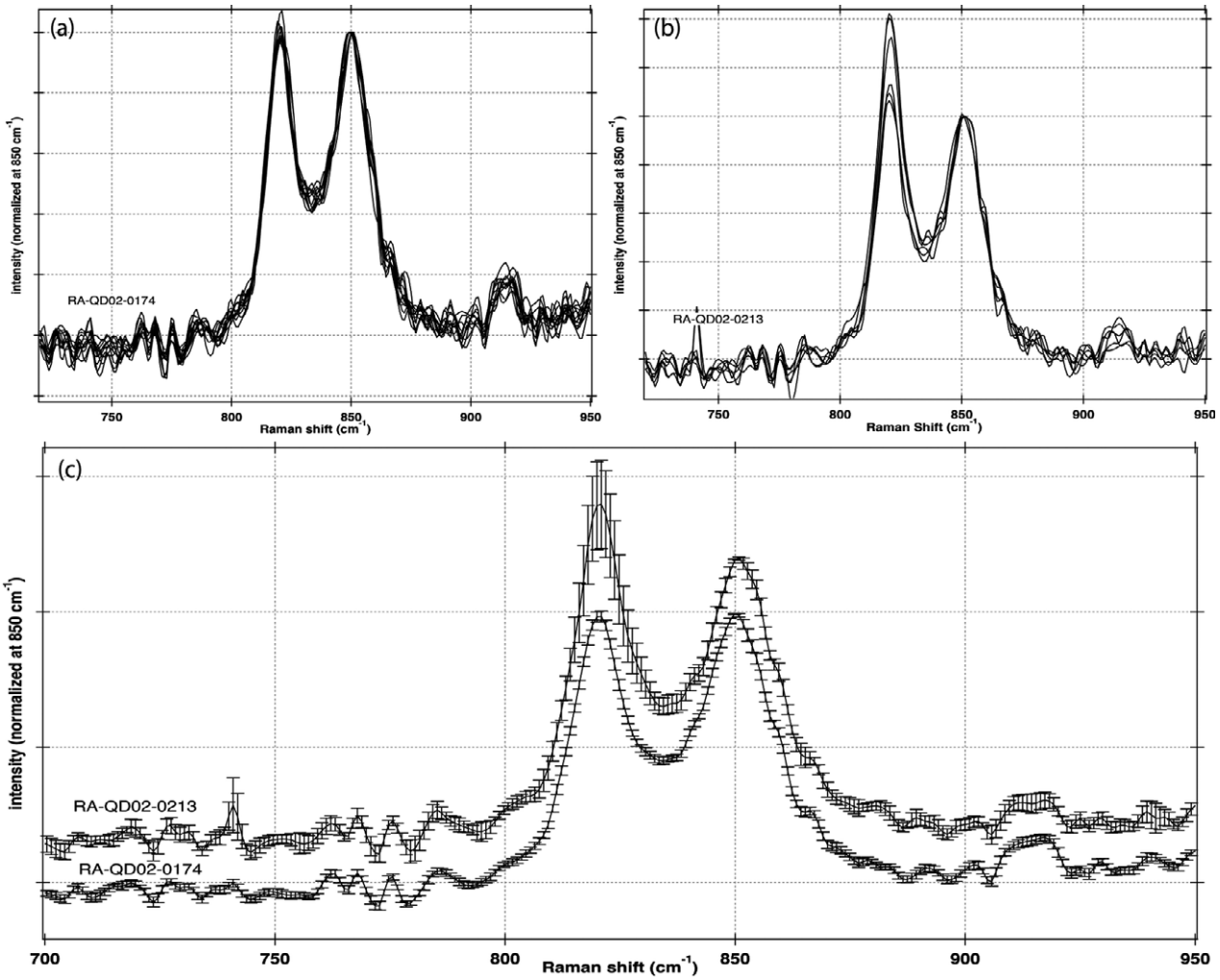

Fig. 4. Raman spectra of RA-QD02-0174 (a) and RA-QD02-0213 (b) and comparison of the average spectra obtained on these two grains, variability shown by the error bars (c). Spectra (a, b) were collected at different locations on each of the grain: they are solely composed of olivine, as attested by the presence of the spectral doublet in ~820–850 cm^{-1} region. The positions of the olivine Raman doublet are similar within each of the grains and also between the grains (c), revealing a homogeneous and similar elemental chemical composition.

we have and is composed of olivine and pyroxene. The chemical compositions of the olivine in RA-QD02-174, RA-QD02-213, and RA-QD02-163 are fairly similar, Mg-rich (Fo_{76}). No oxide, hydrated minerals, plagioclase, or carbon-rich grains were detected. The mineralogy of these three Itokawa particles is consistent with previously characterized particles (e.g., Nakamura et al. 2011).

Major minerals in equilibrated ordinary chondrites are olivine, low-Ca pyroxene, and Fe,Ni-metal (Brearley and Jones 1998). Plagioclase, diopside, and troilite are minor minerals. The elemental compositions and relative abundances of the major minerals are used to classify ordinary chondrites into H, L, and LL groups (e.g., Rubin 1990; Brearley and Jones 1998). Olivine composition, is $Fo_{68\text{-}74}$ for LL chondrites, $Fo_{74\text{-}79}$ for L chondrites, and $Fo_{80\text{-}84}$ for H chondrites (e.g., Kallemeyn et al. 1989). Close examination of mineral chemistries in 38 Hayabusa particles by Nakamura et al. (2011) revealed two different populations: poorly and highly equilibrated particles. The poorly equilibrated particles contain olivine with compositional range $Fa_{24.4\text{-}28.9}$ (i.e., $Fo_{69.7\text{-}75.6}$); the highly equilibrated particles have narrower olivine compositional range with $Fa_{27.1\text{-}30.7}$ (i.e., $Fo_{69.3\text{-}72.9}$). This suggests that the Hayabusa particles considered in the present paper are characterized by a compositional range of the olivine minerals similar to the least equilibrated Hayabusa particles and are related to L/LL chondrites.

Among the mineralogical parameters used to characterize thermal metamorphism of ordinary chondrites, the ones applicable to the Hayabusa particles are the compositional ranges of major minerals

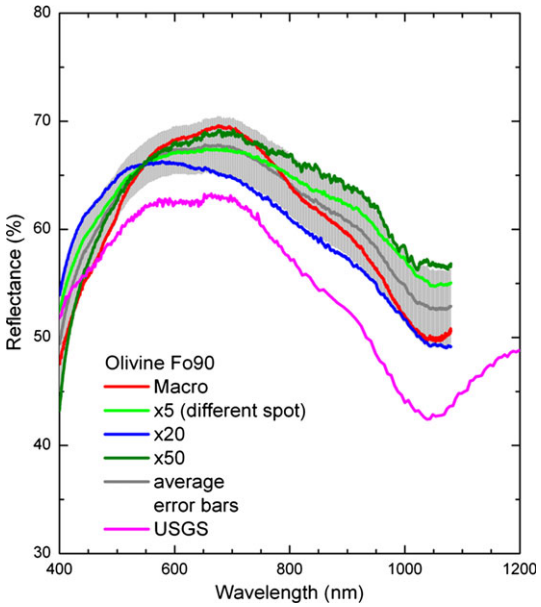

Fig. 5. VIS-NIR bidirectional (i = 45°; e = 0°) reflectance spectra of San Carlos olivine. Spectra acquired using different microscope objectives (×20 and ×50 in blue and green on one specific grain of about 40 μm in size, and ×5 in light green on a bigger grain of 100 μm in size) are compared with that of "macroscopic" dust (in red, see VIS-NIR section). A spectrum (in pink) obtained from the USGS Spectral Library (Clark et al. 2003) of an olivine of similar composition (Fo_{90}) but of different origin (Twin Sisters Peak, Washington), acquired with a different viewing geometry (directional-conical, with an average angle of 30°), is also shown for comparison. Errors bars relative to the average spectrum are shown in light gray.

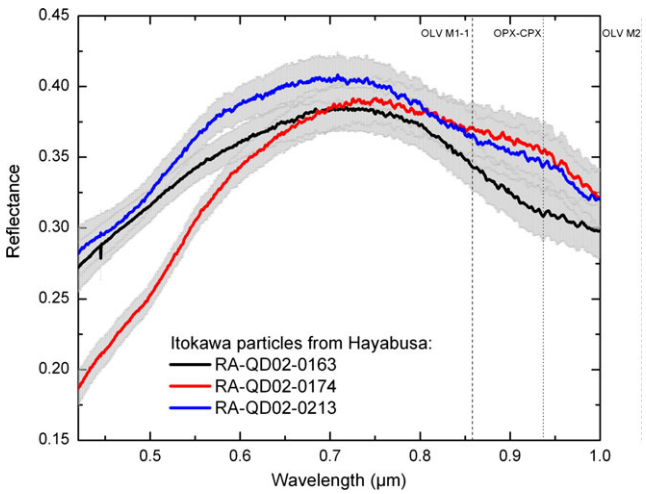

Fig. 6. The VIS-NIR bidirectional (i = 45°; e = 0°) reflectance spectra of Itokawa particles −0163, −0174, and −0213 and their respective error bars (light gray). Vertical lines, around 0.86 μm and 0.94 μm, show the positions (retrieved from the literature) of bands M1-1 and M2 of a Fo_{75} olivine (dashed lines; Sunshine and Pieters 1998) and of the large ~0.94 μm band of a mixture 50:50 of orthopyroxene and clinopyroxene (dotted lines; Sunshine et al. 1990).

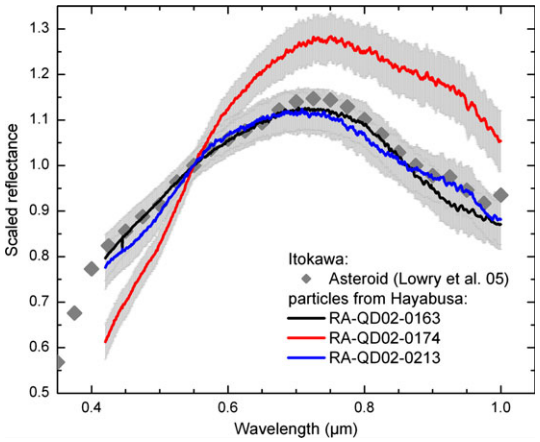

Fig. 7. Comparison of the reflectance spectra of the three Itokawa particles (solid lines) considered in this study with the ground-based observed spectrum of the asteroid Itokawa (dots, from Lowry et al. 2005). Spectra are scaled to unity at 0.55 μm. Differences in the 1 μm band between Itokawa's and the particle's spectra (−163 and −213) could be due to a different olivine/pyroxene ratio. Unfortunately, the limited spectral range does not allow for a more detailed study of the 1 μm band.

Table 1. Visible-NIR spectral slopes calculated from spectra normalized at 0.55 μm, for asteroid Itokawa, the three particles of this study, and LL5 Alta'ameem for comparison. The two methods differ by the spectral range considered to calculate the slope. The first method (0.4–0.7 μm) is more sensitive to the effects of space weathering than the second one (0.52–0.92 μm). However, the second method is used for comparison with large asteroid spectral database (Lazzarin et al. 2006).

Object	Slope (0.4–0.7 μm range)	Slope (0.52–0.92 μm range)
LL5 Alta'ameem	0.60 ± 0.07 μm^{-1}	−0.54 ± 0.05 μm^{-1}
Itokawa	1.22 ± 0.20 μm^{-1}	−0.04 ± 0.15 μm^{-1}
RA-QD02-0163	1.19 ± 0.10 μm^{-1}	0.04 ± 0.07 μm^{-1}
RA-QD02-0213	1.38 ± 0.10 μm^{-1}	0.03 ± 0.07 μm^{-1}
RA-QD02-0174	2.54 ± 0.10 μm^{-1}	0.79 ± 0.07 μm^{-1}

and abundance ratio of orthopyroxene to clinopyroxene. Indeed, as the degree of metamorphism increases, the chemical composition of olivine and pyroxene becomes more homogeneous and the FeO content increases. Moreover, during thermal metamorphism, clinopyroxene is progressively transformed to orthopyroxene. The polymineralic Hayabusa particle RA-QD02-0163 exhibits ortho- and clinopyroxene. It is thus among the least metamorphosed particles brought back from the surface of the Itokawa asteroid and can be related to L/LL4 ordinary chondrites.

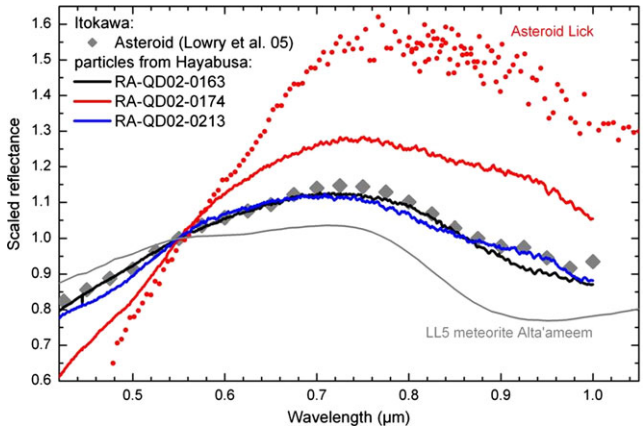

Fig. 8. Comparison of the reflectance spectra of objects having experienced distinct extents of space weathering: our three Hayabusa particles (in black, blue and red), the ground-based spectra of asteroids Itokawa (in gray diamonds) and Lick (in red dots), and the laboratory spectrum of the Alta'ameem LL5 meteorite (in gray line) reported by Hiroi et al. (2006).

Reflectance Spectroscopy and Space Weathering

The understanding of the link between asteroids and meteorites is largely based on the comparison of their respective reflectance spectra. Although ordinary chondrites have been related to Q- and S-type asteroids since the 1990s (e.g., Gaffey et al. 1993), there is no perfect match between their respective reflectance spectra (e.g., Binzel et al. 2001). This discrepancy is now interpreted as related to distinct intensities of space weathering. The effect of various intensities of space weathering on the reflectance spectra is visible when comparing (Fig. 8) the normalized spectra of the three Hayabusa particles to those of a weathered asteroidal surface (Lick; Brunetto et al. 2007a), to an LL5 ordinary chondrite (Alta'ameem meteorite, RELAB database), and to ground-based observations of Itokawa (Lowry et al. 2005). Lick is chosen because it is one of the reddest asteroids in the solar system. The Alta'ameem meteorite is often used as an appropriate analog for a nonweathered surface in the case of Itokawa (e.g., Hiroi et al. 2006). The reflectance spectra of the three Hayabusa particles are characterized by spectral slopes that are intermediate between those for nonweathered (Alta'ameem) and very mature (Lick) surfaces. The observed spectral colors may be related to the presence of nanophase metallic iron and/or nanophase iron sulfides, by-products of space weathering induced by solar wind. Nanophase metallic iron and iron sulfides (FeS) have been detected on other Itokawa particles (Noguchi et al. 2011, 2014).

The reflectance spectrum of particle RA-QD02-0174 has a similar 1 μm band depth but a significantly redder spectral slope than RA-QD02-0163 and RA-QD02-0213 and asteroid Itokawa (see Table 1). This strongly suggests that RA-QD02-174 has endured a higher extent of space weathering. The abundance of nanophase metallic iron and FeS in RA-QD02-0174 may be larger than that in the average surface grains (to be confirmed by different and independent techniques). A variable intensity of space weathering experienced by grains coming from the surface of the same asteroidal object is not surprising and can be explained by a regolith motion scenario. Shestopalov et al. (2013) recently showed that efficient optical alteration induced by space weathering (on short timescales) may be counterbalanced by small impacts and impact-activated motion of regolith. The thin regolith at the surface of Itokawa is composed of loose and mobile grains. Some particles may thus have been more or less exposed to space weathering, leading to a range of optical alteration. As discussed in the next paragraph, the differences among the grains can be interpreted in terms of the history of the Itokawa asteroid.

Spectral Modeling and Timescales

Based on experiments and observations, it is known that space weathering induces changes mainly in the spectral continuum above bands, while it does not affect the band position and VIS-NIR silicate absorptions features (see e.g., Gaffey [2010]; and references therein). The "weathered component" of the spectral continuum is a nonlinear function of the optical constants of the silicate host matrix and of the inclusions produced by the energetic alteration (Hapke 2001; Hiroi and Sasaki 2001; Hiroi et al. 2006; Brunetto et al. 2006b, 2007b; Noble et al. 2007). Hapke (2001) developed a model to describe space weathering, considering the formation of metallic iron particles (smaller than the wavelength) in vapor-deposited coatings on soil particle surfaces and inside agglutinates (i.e., composite mixtures of smaller particles of minerals and glass weakly sintered together; Hapke 2001). This process has been studied by observing the correlation between the abundance of surface deposits of nanophase iron and the variations of optical properties of lunar soils (Pieters et al. 2000). Several laboratory results showed the formation of iron nanoparticles in space weathering experiments (Sasaki et al. 2001; Loeffler et al. 2009; Brunetto et al. 2006a). The recent discovery of the multilayer structure on Itokawa particles associated with space weathering (Noguchi et al. 2014) and the presence of nanophase FeS will likely provide fundamental inputs in the developments of a new and improved space weathering model for asteroids in the near future. Improved versions of the Hapke space weathering model have been developed by Nimura et al. (2008) and by Lucey

and Riner (2011). These more recent models are able to account for any abundance and size variations of the nanophase iron, and they are appropriate for objects having heavily weathered surfaces such as the Moon and Mercury. For objects having relatively low abundance of nanophase iron (such as asteroid Itokawa), the Hapke (2001) version remains a valuable model, as it has been shown by Hiroi et al. (2006). Here we explore the possibility to perform VIS-NIR diffuse reflectance spectra of isolated Itokawa particles to be compared with remote sensing spectral data. Thus, for simplicity, in the following we used the Hapke (2001) spectral model to estimate the difference in abundance of nanophase iron between the Hayabusa particles RA-QD02-0163, RA-QD02-0213, and RA-QD02-0174.

In Hapke's space weathering model, the Maxwell-Garnett effective medium theory is used to calculate the absorption coefficient of a silicate host medium containing inclusions of small metallic iron spheres. In the model, this homogeneous medium is then used as a coating layer on top of unaltered materials. The resulting absorption coefficient $\alpha(\lambda)$ of a material containing metallic iron particles can be written as:

$$\alpha(\lambda) = \alpha_h(\lambda) + 36\pi\varphi z(\lambda)/\lambda \quad (1)$$

where λ is the wavelength, $\alpha_h(\lambda)$ is the absorption coefficient of the host silicate matrix, φ is the volume fraction of metallic iron particles in the host matrix and is a function of the concentration of inclusions and relative densities of inclusion and host materials. The function $z(\lambda)$ is given by:

$$z(\lambda) = (n_h^3 n_{Fe} k_{Fe})/[(n_{Fe}^2 - k_{Fe}^2 + 2n_h^2) + (2n_{Fe}k_{Fe})^2] \quad (2)$$

where n_h is the real part of the refractive index of the host material, n_{Fe} and k_{Fe} are the real and imaginary parts of the refractive index of iron. An example of Hapke's space weathering model applied to asteroid Itokawa is provided by Hiroi et al. (2006) in the NIR spectral region. Hiroi et al. (2006) assumed that the absorbance spectrum of the asteroid can be approximated by the negative natural logarithm of its reflectance spectrum $R(\lambda)$:

$$\ln R(\lambda) \approx -\{\alpha_h(\lambda) + 36\pi\varphi\, z(\lambda)/\lambda\} d_e \quad (3)$$

where d_e is the mean optical path length. In the case $\varphi = 0$ (no iron inclusions), Equation 3 gives an estimate of $\alpha_h(\lambda)$ once the reflectance spectrum is measured and the effective grain size is estimated.

We first applied Equation 3 to the Itokawa visible spectrum (Lowry et al. 2005), starting from the Alta'ameem spectrum and assuming that this meteorite has a composition similar to that of the asteroid (as in Hiroi et al. 2006). We assumed $n_h = 1.66$ (a reasonable intermediate value between about 1.67–1.68 for olivine and 1.65 for pyroxene optical constants) and we used the optical constants of iron from Johnson and Christy (1974) for n_{Fe} and k_{Fe}. We obtained a satisfactory fit using a mean optical path length and a volume fraction of metallic iron particles of $d_e = 30$ μm and $\varphi = 0.056\%$, respectively. These values are compatible with the findings of Hiroi et al. (2006) using Hayabusa's NIRS spectra ($d_e = 39.6$ μm and $\varphi = 0.031\%$ for bright areas; $d_e = 27.6$ μm and $\varphi = 0.069\%$ for dark areas on Itokawa's surface). According to such a model, particles RA-QD02-0163 and RA-QD02-0213 would have similar nanophase iron abundance to asteroid Itokawa within the spectral error bars.

The same model was applied to particle RA-QD02-0174, characterized by a distinct reflectance spectrum (Fig. 8). The spectrum of Alta'ameem did not provide a satisfactory fit for particle RA-QD02-0174, mainly because of a marked 0.60–0.65 μm band in the spectrum of the meteorite, attributed to enstatite that is not detected in the spectrum of RA-QD02-0174, and because of a different shape of the left wing of 1 μm band. Using a nonweathered (using Equation 3) spectrum of Itokawa as starting composition for RA-QD02-0174, we obtained the result shown in Fig. 9. The model provides a reasonable fit (within the experimental spectral error bars) using $d_e = 30$ μm and $\varphi = 0.11\%$. Using a deweathered spectrum of RA-QD02-0213 as starting composition for RA-QD02-0174 (both particles are dominated by olivine) produced similar results. In other words, the abundance of nanophase iron in particle RA-QD02-0174 is probably twice as high as the average of Itokawa's surface ($\varphi = 0.11\%$ versus $\varphi = 0.031$–0.069%, respectively).

That semi-quantitative approach is in agreement with the interpretation, based on their respective reflectance spectra exposed above, that particle RA-QD02-0174 is more space weathered than particles RA-QD02-0213 and RA-QD02-0163.

Changes in the optical properties of a planetary surface, darkening and reddening along with subdued absorption bands, are induced by micrometeorite impacts and irradiation by solar wind. Previous studies have found that the time scale for micrometeorite impacts to cause changes in the optical properties of a S-type planetary surface is about 10^8–10^9 yr (Sasaki et al. 2001; Brunetto et al. 2006b). However, effects of solar wind are visible on a much shorter time scale of 10^4–10^5 yr (Hapke 2001; Strazzulla et al. 2005). Studying young asteroid families (<1 Myr), Vernazza et al. (2009) showed that for the asteroidal environment

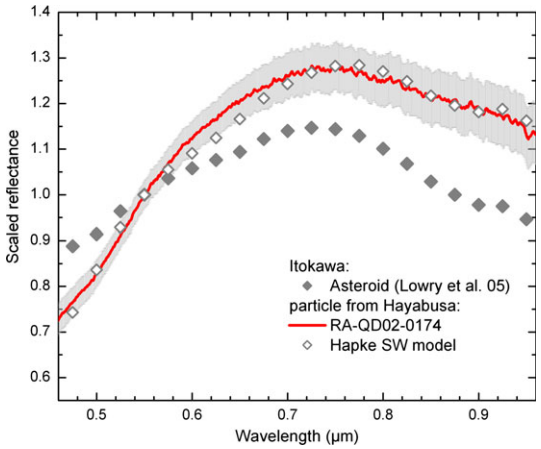

Fig. 9. Hapke (2001) space weathering model (white diamonds) applied to particle RA-QD02-0174 (in red) using a deweathered asteroid Itokawa spectrum (gray diamonds) as pristine composition.

space weathering is a rapid alteration process consistent with solar wind bombardment simulation time scale.

To estimate a weathering time scale corresponding to the reddening observed on the three Itokawa particles, we use the measurements and model of Brunetto et al. (2006a), where the spectral reddening is an exponential function of a C_S parameter directly related to the irradiation dose. Brunetto et al. (2006a) found that the VIS-NIR reddening and darkening process mainly affects the continuum of reflectance spectra. This continuum can be parameterized by a C_S coefficient: spectral continuum = $K \exp(C_S/\lambda)$, where K is a scale factor that changes according to the normalization of the spectra. The C_S parameter is strongly related with the number of displacements per unit area (d, damage parameter) after irradiation with heavy ions: $C_S = \alpha \ln(\beta d + 1)$, where $\alpha = -0.33 \pm 0.06$ μm and $\beta = (1.1 \pm 0.5) \times 10^{-19}$ cm^2. The damage value d corresponds to a given exposure time in space, once the ion fluxes and energies of a given astronomical environment are known (see Brunetto et al. [2006a] for details about the estimation of the timescales). Using the slope of the Alta'ameem meteorite for the unweathered starting point, we find $C_S = -0.2$ (± 0.05) μm for particles RA-QD02-0163 and RA-QD02-0213, and $C_S = -0.5$ (± 0.05) μm for particle RA-QD02-0174. Considering only heavy ions (see discussion in Brunetto et al. 2006a) we infer timescales of about 2×10^6 yr for particles RA-QD0200163 and RA-QD02-0213, and 8×10^6 yr for RA-QD02-0174. These values are upper limits, as the timescales may be one or two orders of magnitude shorter due to irradiation with hydrogen and helium instead of heavy ions (see Hapke 2001). In any case, the relative timescale difference remains the same, i.e., the particle RA-QD02-0174 has been exposed to the solar ion flux for a duration ~4 times longer than particles RA-QD02-0163 and RA-QD02-0213.

The relative short residence times estimated for Itokawa's particles (Nagao et al. 2011; Keller and Berger 2014; Noguchi et al. 2014), the relatively red VIS-NIR spectra presented in this work, and the weathering timescales previously estimated through distinct laboratory experiments (e.g., Sasaki et al. 2001; Brunetto et al. 2006b) confirm that solar ion irradiation (and not micrometeorite bombardment) is the main cause for rapid asteroidal space weathering, as demonstrated by Vernazza et al. (2009).

CONCLUSIONS

We have characterized the mineralogy of individual raw grains through nondestructive Raman spectroscopy. RA-QD02-0163, RA-QD02-0174, and RA-QD02-0213 are related to equilibrated L/LL4 chondrites. Visible-NIR reflectance spectra on the three allocated individual grains are consistent with those of the Itokawa asteroidal surface. The differences in spectral slope in the reflectance spectra of the three particles are interpreted in terms of variations in the intensity of space weathering experienced by each of the particles. RA-QD02-0174 appears to be the most space weathered.

To go further in the characterization of space weathering and to better constrain the link between the spectral slope of reflectance spectra and the abundance of Fe-rich nanoparticles, additional analytical techniques, such as STEM, need to be applied to image the npFe^0. Interestingly, the two touchdown locations of the Hayabusa spacecraft are approximately 100 m apart on the Itokawa asteroid. Considering the topography near the sampling site (Yano et al. 2006), the regolith at the first touchdown site (particles from room B) may be more affected by space weathering than the regolith at the second touchdown site (particles from room A). It would be worth acquiring the reflectance spectra of particles from room B to compare to those of the present study (room A). This would allow better assessment of the variability in space weathering at the surface of airless bodies.

A key scientific objective of the present consortium is to measure the abundances of noble gases in the individual particles, requiring whole grains analysis. We thus could not further investigate the abundance of iron nanoparticles in the three allocated particles. The upcoming noble gas analyses will allow us to quantify the proportion of solar and cosmogenic volatiles in these Itokawa samples, and to better constrain the residence time of dust particles at the surface of the

asteroid. The cosmic-ray exposure age of the three Itokawa particles, derived from the abundance of cosmogenic noble gas nuclides (e.g., ^{21}Ne and ^{38}Ar), can then be compared to the timescales of space weathering determined here. Ultimately, the link between physical and chemical data will help our understanding of the evolution of the Itokawa asteroid.

Acknowledgments—The Hayabusa-returned samples RA-QD02-0163, RA-QD02-0174, and RA-QD02-0213 were allocated by JAXA's Extraterrestrial Sample Curation Team (ESCuTe) through the first International Announcement of Opportunity. We also thank the local organizing committee of the 1st international Hayabusa symposium, the Extraterrestrial Sample Curation Team (ESCute) of JAXA, in October 2013, where multiple discussions helped in the writing of the present paper. We are grateful to P. Dumas and C. Sandt for help and support at the SMIS beamline. This research is part of the INGMAR project and it has been funded by the French national program "Programme National de Planétologie" (PNP), by the Faculté des Sciences d'Orsay, Université Paris-Sud ("Attractivité 2012"), by the French "Agence Nationale de la Recherche" (contract ANR-11-BS56-0026, OGRESSE), and by the P2IO LabEx (ANR-10-LABX-0038) in the framework "Investissements d'Avenir" (ANR-11-IDEX-0003-01) managed by the French National Research Agency (ANR). The Raman facility in Lyon is supported by the Institut National des Sciences de l'Univers.

Editorial Handling—Dr. Michael Gaffey

REFERENCES

Abe M., Takagi Y., Kitazato K., Abe S., Hiroi T., Vilas F., Clark B. E., Abell P. A., Lederer S. M., Jarvis K. S., Nimura T., Ueda Y., and Fujiwara A. 2006. Near-infrared spectral results of asteroid Itokawa from the Hayabusa spacecraft. *Science* 312:1334–1338.

Abell P. A., Vilas F., Jarvis K. S., Gaffey M. J., and Kelley M. S. 2007. Mineralogical composition of (25143) Itokawa 1998 SF36 from visible and near-infrared reflectance spectroscopy: Evidence for partial melting. *Meteoritics & Planetary Science* 42:2165–2177.

Basu A. and McKay A. S. 1983. Rarity of lunar soil analogs in meteorites. *Meteoritics* 18:263.

Bennett C. J., Pirim C., and Orlando T. M. 2013. Space-weathering of solar system bodies: A laboratory perspective. *Chemical Reviews* 113:9086–9150.

Binzel R. P., Rivkin A. S., Bus J. S., Sunshine J. M., and Burbine T. H. 2001. MUSES-C target asteroid (25143) 1998 SF36: A reddened ordinary chondrite. *Meteoritics & Planetary Science* 36:1167–1172.

Binzel R. P., Rivkin A. S., Stuart J. S., Harris A. W., Bus S. J., and Burbine T. H. 2004. Observed spectral properties of near-Earth objects: Results for population distribution, source regions, and space weathering processes. *Icarus* 170:259–294.

Brearley A. J. and Jones R. H. 1998. Chondritic meteorites. *Reviews in Mineralogy* 36:3.1–3.370.

Brunetto R., Vernazza P., Marchi S., Birlan M., Fulchignoni M., Orofino V., and Strazzulla G. 2006a. Modeling asteroid surfaces from observations and irradiation experiments: The case of 832 Karin. *Icarus* 184:327–337.

Brunetto R., Romano F., Blanco A., Fonti S., Martino M., Orofino V., and Verrienti C. 2006b. Space weathering of silicates simulated by nanosecond pulse UV excimer laser. *Icarus* 180:546–554.

Brunetto R., de Leòn J., and Licandro J. 2007a. Testing space weathering models on A-type asteroid (1951) Lick. *Astronomy & Astrophysics* 472:653–656.

Brunetto R., Roush T. L., Marra A. C., and Orofino V. 2007b. Optical characterization of laser ablated silicates. *Icarus* 191:381–393.

Brunetto R., Borg J., Dartois E., Rietmeijer F. J. M., Grossemy F., Sandt C., Le Sergeant d'Hendecourt L., Rotundi A., Dumas P., Djouadi Z., and Jamme F. 2011. Mid-IR, far-IR, Raman micro-spectroscopy, and FESEM-EDX study of IDP L2021C5: Clues to its origin. *Icarus* 212:896–910.

Brunetto R., Lantz C., Ledu D., Baklouti D., Barucci M. A., Beck P., Delauche L., Dionnet Z., Dumas P., Duprat J., Engrand C., Jamme F., Oudayer P., Quirico E., Sandt C., and Dartois E. 2014. Ion irradiation of Allende meteorite probed by visible, IR, and Raman spectroscopies. *Icarus* 237:278–292.

Brunetto R., Loeffler M. J., Nesvorný D., Sasaki S., and Strazulla G. 2015. Asteroid surface alteration by space weathering processes. In *Asteroid IV*, edited by Michel P., DeMeo F. E., and Bottke W. F. Tucson, Arizona: The University of Arizona Press.

Cassidy W. and Hapke B. 1975. Effects of darkening processes on surfaces of airless bodies. *Icarus* 25:371–383.

Chapman C. R. 1996. S-type asteroids, ordinary chondrites, and space weathering: The evidence from Galileo's fly-bys of Gaspra and Ida. *Meteoritics & Planetary Science* 31:699–725.

Chapman C. R. 2004. Space weathering of asteroid surfaces. *Annual Review of Earth and Planetary Sciences* 32:539–567.

Clark B. E., Hapke B., Pieters C., and Britt D. 2002. *Asteroid space weathering and regolith evolution*. *Asteroid III*. Tucson, Arizona: Univeristy of Arizona Press. pp. 585–599.

Clark R. N., Swayze G. A., Wise R., Livo K. E., Hoefen T. M., Kokaly R. F., and Sutley S. J. 2003. USGS Digital Spectral Library splib05a. USGS Open File Report, 03-395. http://pubs.usgs.gov/of/2003/ofr-03-395/ofr-03-395.html

Dartois E., Engrand C., Brunetto R., Duprat J., Pino T., Quirico E., Remusat L., Bardin N., Briani G., Mostefaoui S., Morinaud G., Crane B., Szwec N., Delauche L., Jamme F., Sandt C., and Dumas P. 2013. Ultracarbonaceous Antarctic micrometeorites, probing the solar system beyond the nitrogen snow-line. *Icarus* 224:243–252.

Domingue D. L., Chapman C. R., Killen R. M., Zurbuchen T. H., Gilbert J. A., Sarantos M., Benna M., Slavin J. A., Schriver D., Trávnícek P. M., Orlando T. M., Sprague A. L., Blewett D. T., Gillis-Davis J. J., Feldman W. C.,

Lawrence D., Ho G. C., Ebel D. S., Nittler L. N., Vilas F., Pieters C. M., Solomon S. C., Johnson C. L., Winslow R. M., Helbert J., Peplowski P. N., Weider S. Z., Mouawad N., Izenberg N. R., and McClintock W. E. 2014. Mercury's weather-beaten surface: Understanding Mercury in the context of lunar and asteroidal space weathering studies. *Space Science Reviews* 181:121–214.

Dukes C. A., Baragiola R. A., and McFadden L. A. 1999. Surface modification of olivine by H^+ and He^+ bombardment. *Journal of Geophysical Research* 104:1865–1872.

Dumas P., Polack F., Lagarde B., Chubar O., Giorgetta J. L., and Lefrançois S. 2006. Synchrotron infrared microscopy at the French Synchrotron Facility SOLEIL. *Infrared Physics and Technology* 49:152–160.

Fujiwara A., Kawaguchi J., Yeomans D. K., Abe M., Mukai T., Okada T., Saito J., Yano H., Yoshikawa M., Scheeres D. J., Barnouin-Jha O., Cheng A. F., Demura H., Gaskell R. W., Hirata N., Ikeda H., Kominato T., Miyamoto H., Nakamura A. M., Nakamura R., Sasak S., and Uesugi K. 2006. The rubble-pile asteroid Itokawa as observed by Hayabusa. *Science* 312:1330–1334.

Gaffey M. J. 2010. Space weathering and the interpretation of asteroid reflectance spectra. *Icarus* 209:564–574.

Gaffey M. J., Burbine T. H., and Binzel R. P. 1993. Asteroid spectroscopy: Progress and perspectives. *Meteoritics* 28:161–187.

Hapke B. 1993. Combined theory of reflectance and emittance spectroscopy. In *Remote geochemical analysis: Elemental and mineralogical composition*, edited by Pieters C. M. and Englert P. A. J. New York: Cambridge University Press. pp. 31–42.

Hapke B. 2001. Space weathering from Mercury to the asteroid belt. *Journal of Geophysical Research* 106:10,039–10,074.

Hendrix A. R. and Vilas F. 2006. The effects of space weathering at UV wavelengths: S-class asteroids. *The Astrophysical Journal* 1396–1404.

Hendrix A. R., Retherford K. D., Randall G. G., Hurley D. M., Feldman P. D., Egan A. F., Kaufmann D. E., Miles P. F., Parker J. W., Horvath D., Rojas P. M., Versteeg M. H., Davis M. W., Greathouse T. K., Mukherjee J., Steffl A. J., Pryor W. R., and Stern S. A. 2012. The lunar far-UV albedo: Indicator of hydration and weathering. *Journal of Geophysical Research* 117:E12001.

Hiroi T. and Sasaki S. 2001. Importance of space weathering simulation products in compositional modeling of asteroids: 349 Dembowska and 446 Aeternitas as examples. *Meteoritics & Planetary Science* 36:1587–1596.

Hiroi T., Abe M., Kitazato K., Abe S., Clark B. E., Sasaki S., Ishiguro M., and Barnouin-Jha O. S. 2006. Developing space weathering on the asteroid 25143 Itokawa. *Nature* 443:56–58.

Huang E., Chen C. H., Huang T., Lin E. H., and Xu J.-A. 2000. Raman spectroscopic characteristics of Mg-Fe-Ca pyroxenes. *American Mineralogist* 85:473–479.

Ishiguro M., Hiroi T., Tholen D. J., Sasaki S., Ueda Y., Nimura T., Abe M., Clark B. E., Yamamoto A., Yoshida F., Nakamura R., Hirata N., Miyamoto H., Yokota Y., Hashimoto T., Kubota T., Nakamura A. M., Gaskell R. W., and Saito J. 2007. Global mapping of the degree of space weathering on asteroid 25143 Itokawa by Hayabusa/AMICA observations. *Meteoritics & Planetary Science* 42:1791–1800.

Johnson P. B. and Christy R. W. 1974. Optical constants of transition metals: Ti, V, Cr, Mn, Fe Co, Ni, and Pd. *Physical Review B* 9:5056.

Kallemeyn G. W., Rubin A. E., Wang D., and Wasson J. T. 1989. Ordinary chondrites: Bulk compositions, classification, lithophile-element fractionations, composition-petrographic type relationships. *Geochimica et Cosmochimica Acta* 53:2747–2767.

Keil K. 1982. Composition and origin of chondritic breccias. In *Workshop on lunar breccias and soils and their meteoritic analogs*, edited by Taylor G. J. and Wilkening L. L. LPI Technical Report 82-02. Houston, Texas: Lunar and Planetary Institute. pp. 65–83.

Keller L. P. and Berger E. L. 2014. A transmission electron microscope study of Itokawa regolith grains. *Earth, Planets and Space* 66:71–78.

Keller L. P. and McKay G. 1993. Discovery of vapor deposits in the lunar regolith. *Science* 261:1305–1307.

Keller L. P. and McKay G. 1997. The nature and origin of rims on lunar regolith grains. *Geochimica et Cosmochimica Acta* 61:2331–2341.

Keller L. P., Wentworth S. J., McKay D. S., Taylor L. A., Pieters C., and Morris R. V. 2000. Space weathering in the fine size fractions of lunar soils: Mare/highland differences (abstract #1655). 31st Lunar and Planetary Science Conference. CD-ROM.

Kuebler K. E., Jolliff B. L., Wang A., and Haskin L. A. 2006. Extracting olivine (Fo-Fa) compositions from Raman spectral peak positions. *Geochimica et Cosmochimica Acta* 70:6201–6222.

Lazzarin M., Marchi S., Moroz L. V., Brunetto R., Magrin S., Paolicchi P., and Strazzulla G. 2006. Space weathering in the main asteroid belt: The big picture. *The Astrophysical Journal* 647:L179–L182.

Lederer S. M., Domingue D. L., Vilas F., Abe M., Farnham T. L., Jarvis K. S., Lowry S. C., Ohba Y., Weissman P. R., French L. M., Fukai H., Hasegawa S., Ishiguro M., Larson S. M., and Takagi Y. 2005. Physical characteristics of Hayabusa target Asteroid 25143 Itokawa. *Icarus* 173:153–165.

Loeffler M. J., Dukes C. A., and Baragiola R. A. 2009. Irradiation of olivine by 4 keV He+: Simulation of space weathering by the solar wind. *Journal of Geophysical Research (Planets)* 114:3003.

Lowry S. C., Weissman P. R., Hicks M. D., Whiteley R. J., and Larson S. 2005. Physical properties of asteroid (25143) Itokawa—Target of the Hayabusa sample return mission. *Icarus* 176:408–417.

Lucey P. G. and Riner M. A. 2011. The optical effects of small iron particles that darken but do not redden: Evidence of intense space weathering on Mercury. *Icarus* 212:451–462.

Marchi S., Brunetto R., Magrin S., Lazzarin M., and Gandolfi D. 2005. Space weathering of near-Earth and main belt silicate-rich asteroids: Observations and ion irradiation experiments. *Astronomy & Astrophysics* 443:769–775.

Marchi S., Paolicchi P., Lazzarin M., and Magrin S. 2006. A general spectral slope-exposure relation for S-type main belt and near-Earth Asteroids. *The Astronomical Journal* 131:1138–1141.

McKay D. S., Heiken G., Basu A., Blandfor G., Simon S., Reedy R., French B., and Papike J. J. 1991. The lunar regolith. In *Lunar sourcebook*, edited by Heiken G. H.,

Vaniman D. T., and French B. M. New York: Cambridge University Press. pp. 285–356.

Meier M. M. M., Alwmark C., Bajt S., Böttger U., Busemann H., Fujiya W., Gilmour J., Heitmann U., Hoppe P., Hübers H.-W., Marone F., Ott U., Pavlov S., Schade U., Spring N., Stampanoni M., and Weber I. 2014. A precise cosmic-ray exposure age for an olivine grain from the surface of near-Earth asteroid (25143) Itokawa (abstract #1247). 45th Lunar and Planetary Science Conference. CD-ROM.

Nagao K., Okazaki R., Nakamura T., Miura Y. N., Osawa T., Bajo K., Matsuda S., Ebihara M., Ireland T. R., Kitajima F., Naraoka H., Noguchi T., Tsuchiyama A., Yurimoto H., Zolensky M. E., Uesugi M., Shirai K., Abe M., Yada T., Ishibashi Y., Fujimura A., Mukai T., Ueno M., Okada T., Yoshikawa M., and Kawaguchi J. 2011. Irradiation history of Itokawa regolith material deduced from noble gases in the Hayabusa samples. *Science* 333:1128–1131.

Nakamura T., Noguchi T., Tanaka M., Zolensky M. E., Kimura M., Tsuchiyama A., Nakato A., Ogami T., Ishida H., Uesugi M., Yada T., Shirai K., Fujimura A., Okazaki R., Sandford S. A., Ishibashi Y., Abe M., Okada T., Ueno M., Mukai T., Yoshikawa M., and Kawaguchi J. 2011. Itokawa dust particles: A direct link between S-type asteroids and ordinary chondrites. *Science* 333:1113–1116.

Nesvorný D., Bottke W. F., Vokrouhlický D., Chapman C. R., and Rafkin S. 2010. Do planetary encounters reset surfaces of near Earth asteroids? *Icarus* 209:510–519.

Nimura T., Hiroi T., and Pieters C. M. 2008. An improved scheme for modeling the reflectance spectra of space-weathered regoliths. *Earth, Planets and Space* 60:271–275.

Noble S. K., Pieters C. M., and Keller L. P. 2007. An experimental approach to understanding the optical effects of space weathering. *Icarus* 192:629–642.

Noble S. K., Keller L. P., and Pieters C. M. 2010. Evidence of space weathering in regolith breccias II: Asteroidal regolith breccias. *Meteoritics & Planetary Science* 45:2007–2015.

Noguchi T., Nakamura T., Kimura M., Zolensky M. E., Tanaka M., Hashimoto T., Konno M., Nakato A., Ogami T., Fujimura A., Abe M., Yada T., Mukai T., Ueno M., Okada T., Shirai K., Ishibashi Y., and Okazaki R. 2011. Incipient space weathering observed on the surface of Itokawa dust particles. *Science* 333:1121–1125.

Noguchi T., Kimura M., Hashimoto T., Konno M., Nakamura T., Zolensky M. E., Okazaki R., Tanaka M., Tsuchiyama A., Nakato A., Ogami T., Ishida H., Sagae R., Tsujimoto S., Matsumoto T., Matsuon J., Fujimura A., Abe M., Yada T., Mukai T., Ueno M., Okada T., Shirai K., and Ishibashi Y. 2014. Space weathered rims found on the surfaces of the Itokawa dust particles. *Meteoritics & Planetary Science* 49:188–214.

Okada T., Shirai K., Yamamoto Y., Arai T., Ogawa K., Hosono K., and Kato M. 2006. X-ray fluorescence spectrometry of asteroid Itokawa by Hayabusa. *Science* 312:1338–1341.

Pieters C. M., Taylor L. A., Noble S. K., Keller L. P., Hapke B., Morris R. V., Allen C. C., McKay D. S., and Wentworth S. 2000. Space weathering on airless bodies: Resolving a mystery with lunar samples. *Meteoritics & Planetary Science* 35:1101–1107.

Rubin A. E. 1990. Kamacite and olivine in ordinary chondrites: Intergroup and intragroup relationships. *Geochimica et Cosmochemica Acta* 54:1217–1232.

Sasaki S., Nakamura K., Hamabe Y., Kurahashi E., and Hiroi T. 2001. Production of iron nanoparticles by laser irradiation in a simulation of lunar-like space weathering. *Nature* 410:555–557.

Shestopalov D. I., Golubeva L. F., and Cloutis E. A. 2013. Optical maturation of asteroid surfaces. *Icarus* 225:781–793.

Strazzulla G., Dotto E., Binzel R., Brunetto R., Barucci M. A., Blanco A., and Orofino V. 2005. Spectral alteration of the Meteorite Epinal (H5) induced by heavy ion irradiation: A simulation of space weathering effects on near-Earth asteroids. *Icarus* 174:31–35.

Sunshine J. M. and Pieters C. M. 1998. Determining the composition of olivine from reflectance spectroscopy. *Journal of Geophysical Research* 103:13,675–13,688.

Sunshine J. M., Pieters C. M., and Pratt S. F. 1990. Deconvolution of mineral absorption bands—An improved approach. *Journal of Geophysical Research* 95:6955–6966.

Taylor L. A., Pieters C. M., Keller L. P., Morris R. V., and McKay D. S. 2001. Lunar mare soils: Space weathering and the major effects of surface-correlated nanophase Fe. *Journal of Geophysical Research* 106:27,985–28,000.

Tsuchiyama A., Uesugi M., Matsushima T., Michikami T., Kadono T., Nakamura T., Uesugi K., Nakano T., Sandford S. A., Noguchi R., Matsumoto T., Matsuno J., Nagano T., Imai Y., Takeuchi A., Suzuki Y., Ogami T., Katagiri J., Ebihara M., Ireland T. R., Kitajima F., Nagao K., Naraoka H., Noguchi T., Okazaki R., Yurimoto H., Zolensky M. E., Mukai T., Abe M., Yada T., Fujimura A., Yoshikawa M., and Kawaguchi J. 2011. Three-dimensinal structure of Hayabusa samples: Origin and evolution of Itokawa regolith. *Science* 333:1125–1128.

Van Schmus W. R. and Wood J. A. 1967. A chemical-petrologic classification for the chondritic meteorites. *Geochimica et Cosmochemica Acta* 31:747–765.

Vernazza P., Binzel R. P., Rossi A., Fulchignoni M., and Birlan M. 2009. Solar wind as the origin of rapid reddening of asteroid surfaces. *Nature* 458:993–995.

Wentworth S. J., Keller L. P., McKay D. S., and Morris R. V. 1999. Space weathering on the moon: Patina on Apollo 17 samples 75075 and 76015. *Meteoritics & Planetary Science* 31:1655.

Willman M., Jedicke R., Nesvorný D., Moskovitz N., Ivezić Ž., and Fevig R. 2008. Redetermination of the space weathering rate using spectra of Iannini asteroid family members. *Icarus* 195:663–673.

Yada T., Fujimara A., Abe M., Nakamura T., Noguchi T., Okazaki R., Nagao K., Ishibashi Y., Shirai K., Zolensky M. E., Sandford S., Okada T., Uesugi M., Karouji Y., Ogawa M., Yakame S., Ueno M., Mukai T., Yoshikawa M., and Kawaguchi J. 2014. Hayabusa-returned sample curation in the Planetary Material Sample Curation Facility in JAXA. *Meteoritics & Planetary Science* 49:135–153.

Yamada M., Sasaki S., Nagahara H., Fujiwara A., Hasegawa S., Yano H., Hiroi T., Ohashi H., and Otake H. 1999. Simulation of space weathering of planet-forming materials: Nanosecond pulse laser irradiation and proton implantation on olivine and pyroxene samples. *Earth, Planets and Space* 51:1255–1265.

Yano H., Kubota T., Miyamoto H., Okada T., Scheeres D., Takagi Y., Yoshida K., Abe M., Abe S., Barnouin-Jha O., Fujiwara A., Hasegawa S., Hashimoto T., Ishiguro M.,

Kato M., Kawaguchi J., Mukai T., Saito J., Sasaki S., and Yoshikawa M. 2006. Touchdown of the Hayabusa spacecraft at the Muses Sea on Itokawa. *Science* 312:1350–1353.

Yurimoto H., Abe K., Abe M., Ebihara M., Fujimura A., Hashiguchi M., Hashizume K., Ireland T. R., Itoh S., Katayama J., Kato C., Kawaguchi J., Kawasaki N., Kitajima F., Kobayashi S., Meike T., Mukai T., Nagao K., Nakamura T., Naraoka H., Noguchi T., Okazaki R., Park C., Sakamoto N., Seto Y., Takei M., Tsuchiyama A., Uesugi M., Wakaki S., Yada T., Yamamoto K., Yoshikawa M., and Zolensky M. E. 2011. Oxygen isotopic compositions of asteroidal materials returned from Itokawa by the Hayabusa missions. *Science* 333:1116–1119.